

PRODUCTION OF HEAVY PARTICLE PAIRS VIA
PHOTON–PHOTON PROCESSES AT THE LHC*

MARTA ŁUSZCZAK

College of Natural Sciences, Institute of Physics, University of Rzeszów
Pigonia 1, 35-310 Rzeszów, Poland

ANTONI SZCZUREK

Institute of Nuclear Physics Polish Academy of Sciences
Radzikowskiego 152, 31-342 Kraków, Poland
andFaculty of Mathematics and Natural Sciences, University of Rzeszów
Pigonia 1, 35-310 Rzeszów, Poland*(Received April 29, 2020)*

We discuss production of W^+W^- pairs and $t\bar{t}$ quark–antiquark pairs in proton–proton collisions induced by two-photon fusion including transverse momenta of incoming photons. The unintegrated inelastic fluxes (related to proton dissociation) of photons are calculated based on modern parametrizations of deep inelastic structure functions in a broad range of x and Q^2 . We focus on processes with single and double proton dissociation. Highly excited remnant systems hadronise producing particles that can be vetoed in the calorimeter. We calculate associated gap survival factors. The gap survival factors depend on the process, mass of the remnant system and collision energy. The rapidity gap survival factor due to remnant fragmentation for double dissociative (DD) collisions is smaller than that for single dissociative (SD) process. We observe approximate factorisation: $S_{R,DD} \approx S_{R,SD}^2$ when imposing rapidity veto. For the W^+W^- final state, the remnant fragmentation leads to a taming of the cross section when the rapidity gap requirement is imposed. Moreover, for $t\bar{t}$ quark–antiquark pairs such a condition reverses the hierarchy observed for the case when such a condition is taken into account. Our results imply that for the production of such heavy objects as t quark and \bar{t} antiquark, the virtuality of the photons attached to the dissociative system is very large ($Q^2 < 10^4 \text{ GeV}^2$). A similar effect is observed for the W^+W^- system.

DOI:10.5506/APhysPolB.51.1449

* Presented at XXVI Cracow Epiphany Conference on LHC Physics: Standard Model and Beyond, Kraków, Poland, January 7–10, 2020

1. Introduction

Photon-induced processes in proton–proton interactions have become very topical recently. Experimentally, they can be separated from other competing processes by imposing rapidity gaps around the electroweak vertex. Both charged lepton pairs l^+l^- [1–5] and electroweak gauge bosons W^+W^- [6, 7] were recently studied experimentally at the Large Hadron Collider. In particular, processes with W^+W^- are of special interest in the context of searches beyond Standard Model [8, 9]. There are, in general, different categories of such processes depending on whether the proton stays intact or undergoes an electromagnetic dissociation (see *e.g.* [10, 11]).

The W^+W^- production in proton–proton processes via the $\gamma\gamma \rightarrow W^+W^-$ subprocess was studied in collinear [12] and transverse momentum dependent factorisation [13] approaches. In our paper [13], we showed that rather large photon virtualities and large mass proton excitation are characteristic for the $\gamma\gamma \rightarrow W^+W^-$ induced processes. Our main aim was to estimate gap survival factor associated with the remnant hadronisation, which destroys the rapidity gap. In [14], we concentrated on the effect related to remnant fragmentation and its destroying of the rapidity gap. Finally, in [15], we calculated cross section for the photon–photon contribution for the $pp \rightarrow t\bar{t}$ reaction including also effects of gap survival probability.

2. A sketch of the formalism

In our analyses of heavy particle pair production via photon–photon processes, we included different categories of processes shown in Fig. 1. In contrast to other authors, our calculations are based on unintegrated inelastic photon fluxes. The unintegrated photon fluxes can be obtained using the following equation:

$$\gamma_{\text{in}}^p(x, \vec{q}_T) = \frac{1}{x} \frac{1}{\pi \vec{q}_T^2} \int_{M_{\text{thr}}^2} dM_X^2 \mathcal{F}_{\gamma^* \leftarrow p}^{\text{in}}(x, \vec{q}_T, M_X^2), \quad (1)$$

and we use the functions $\mathcal{F}_{\gamma^* \leftarrow p}^{\text{in}}$

$$\mathcal{F}_{\gamma^* \leftarrow p}^{\text{in}}(x, \vec{q}_T) = \frac{\alpha_{\text{em}}}{\pi} \left\{ (1-x) \left(\frac{\vec{q}_T^2}{\vec{q}_T^2 + x(M_X^2 - m_p^2) + x^2 m_p^2} \right)^2 \frac{F_2(x_{\text{Bj}}, Q^2)}{Q^2 + M_X^2 - m_p^2} + \frac{x^2}{4x_{\text{Bj}}^2} \frac{\vec{q}_T^2}{\vec{q}_T^2 + x(M_X^2 - m_p^2) + x^2 m_p^2} \frac{2x_{\text{Bj}} F_1(x_{\text{Bj}}, Q^2)}{Q^2 + M_X^2 - m_p^2} \right\}. \quad (2)$$

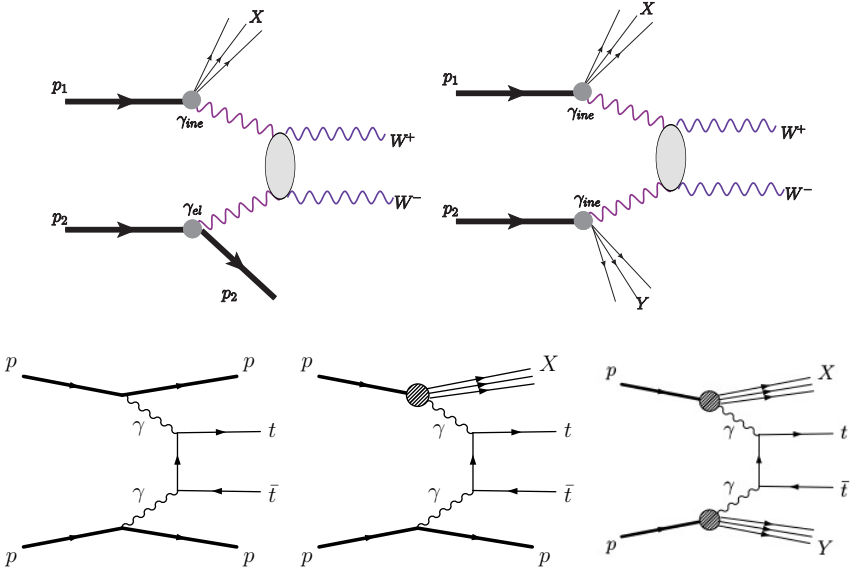


Fig. 1. Diagrams representing different categories of photon–photon-induced mechanisms for production of W^+W^- pairs (top panel) and for production of $t\bar{t}$ pairs (bottom panel).

The virtuality Q^2 of the photon depends on the photon transverse momentum (\vec{q}_T^2) and the proton remnant mass (M_X)

$$Q^2 = \frac{\vec{q}_T^2 + x(M_X^2 - m_p^2) + x^2 m_p^2}{(1-x)}. \quad (3)$$

The proton structure functions $F_1(x_{Bj}, Q^2)$ and $F_2(x_{Bj}, Q^2)$ depend on

$$x_{Bj} = \frac{Q^2}{Q^2 + M_X^2 - m_p^2}. \quad (4)$$

In Eq. (2) we use both $F_2(x_{Bj}, Q^2)$ and $F_L(x_{Bj}, Q^2)$, where

$$F_L(x_{Bj}, Q^2) = \left(1 + \frac{4x_{Bj}^2 m_p^2}{Q^2}\right) F_2(x_{Bj}, Q^2) - 2x_{Bj} F_1(x_{Bj}, Q^2) \quad (5)$$

is the longitudinal structure function of the proton.

The photon fluxes enter the $pp \rightarrow X + (\gamma^* \gamma^\alpha st \rightarrow W^+W^-Y$ and the $p + p \rightarrow X + (\gamma^* \gamma^* \rightarrow t\bar{t}) + Y$ production cross section. Details of the cross-sections calculations are presented in our original papers [13–15].

3. Results for W^+W^- pairs production

Before studying the hadron level, we calculated the gap survival factor on the parton level. In such a case, it is the outgoing parton (jet or mini-jet) which is struck by the virtual photon and destroys the rapidity gap.

The gap survival factor can be then defined as

$$S_R(\eta_{\text{cut}}) = 1 - \frac{1}{\sigma} \int_{-\eta_{\text{cut}}}^{\eta_{\text{cut}}} \frac{d\sigma}{d\eta_{\text{jet}}} d\eta_{\text{jet}}, \quad (6)$$

where $d\sigma/d\eta_{\text{jet}}$ is the rapidity distribution of the cross section for W^+W^- production as a function of rapidity of the extra jet (*de facto* parton) and σ is the associated integrated cross section. In Fig. 2, we show $d\sigma/d\eta_{\text{jet}}$ as a function of η_{jet} . No extra cuts are imposed here. We get a very broad distribution in η_{jet} (see the solid line).

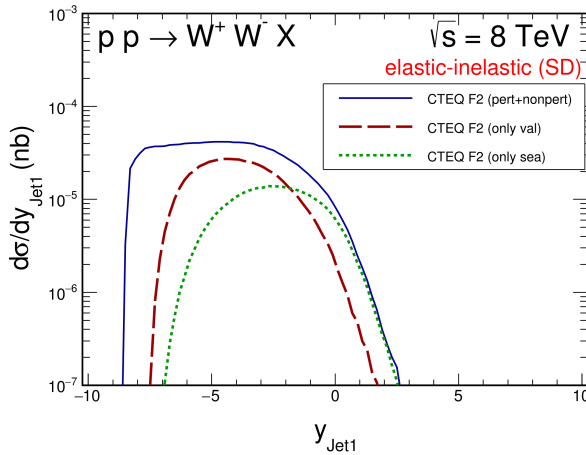


Fig. 2. Jet rapidity distribution using a LO partonic distribution at large Q^2 . The solid line is a sum of all contributions. The dashed line is for the valence component and the dotted line is for the sea component.

We also presented the parton level gap survival factor as a function of the size of the window $(-\eta_{\text{cut}}, \eta_{\text{cut}})$, which is free of the outgoing parton (jet). We show corresponding $S_R(\eta_{\text{cut}})$ in Fig. 3. The solid line represents our partonic result. For comparison, we show also S_R when only one component (valence or sea) of F_2 is included in the calculation, see dashed and dotted lines. We see that gap survival factors for the different components are fairly different. Our final result (solid line) correctly includes all components.

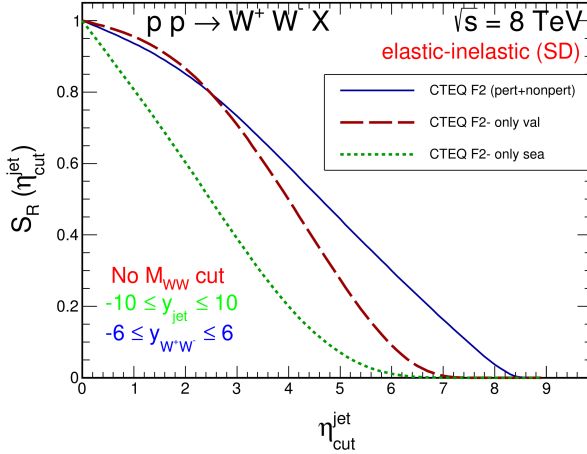


Fig. 3. Gap survival factor associated with the jet emission. The solid line is for the full model, the dashed line for the valence contribution and the dotted line for the sea contribution.

The distribution of S_R for the full model (solid curve) extends to much larger η_{cut} than the valence and sea contributions, separately. This is due to a nonperturbative contribution, which dominates at very large negative rapidities (see the η_{jet} distribution in Fig. 2). The emitted jets can be associated only with the partonic component of the model structure function.

In Fig. 4, we show two-dimensional distributions in pseudorapidity of particles from $X(\eta_X^{\text{ch}})$ and $Y(\eta_Y^{\text{ch}})$ for different ranges of masses of the centrally produced system. For illustration, the region relevant for ATLAS and CMS pseudorapidity coverage is pictured by the thin dashed square.

The two-dimensional plots are not sufficient to see the dependence of the associated gap survival factor on the mass of the centrally produced system.

TABLE I

Average rapidity gap survival factor related to remnant fragmentation for *single dissociative* and *double dissociative* contributions for different ranges of M_{WW} . All uncertainties are statistical only.

Contribution	$S_{R,SD}(\eta^{\text{ch}} < 2.5)$		$(S_{R,SD})^2(\eta^{\text{ch}} < 2.5)$		$S_{R,DD}(\eta^{\text{ch}} < 2.5)$	
	8 TeV	13 TeV	8 TeV	13 TeV	8 TeV	13 TeV
$(2M_{WW}, 200 \text{ GeV})$	0.763(2)	0.769(2)	0.582(4)	0.591(4)	0.586(1)	0.601(2)
$(200, 500 \text{ GeV})$	0.787(1)	0.799(1)	0.619(2)	0.638(2)	0.629(1)	0.649(1)
$(500, 1000 \text{ GeV})$	0.812(2)	0.831(2)	0.659(3)	0.691(3)	0.673(2)	0.705(2)
$(1000, 2000 \text{ GeV})$	0.838(7)	0.873(5)	0.702(12)	0.762(8)	0.697(5)	0.763(6)
Full range	0.782(1)	0.799(1)	0.611(2)	0.638(2)	0.617(1)	0.646(1)

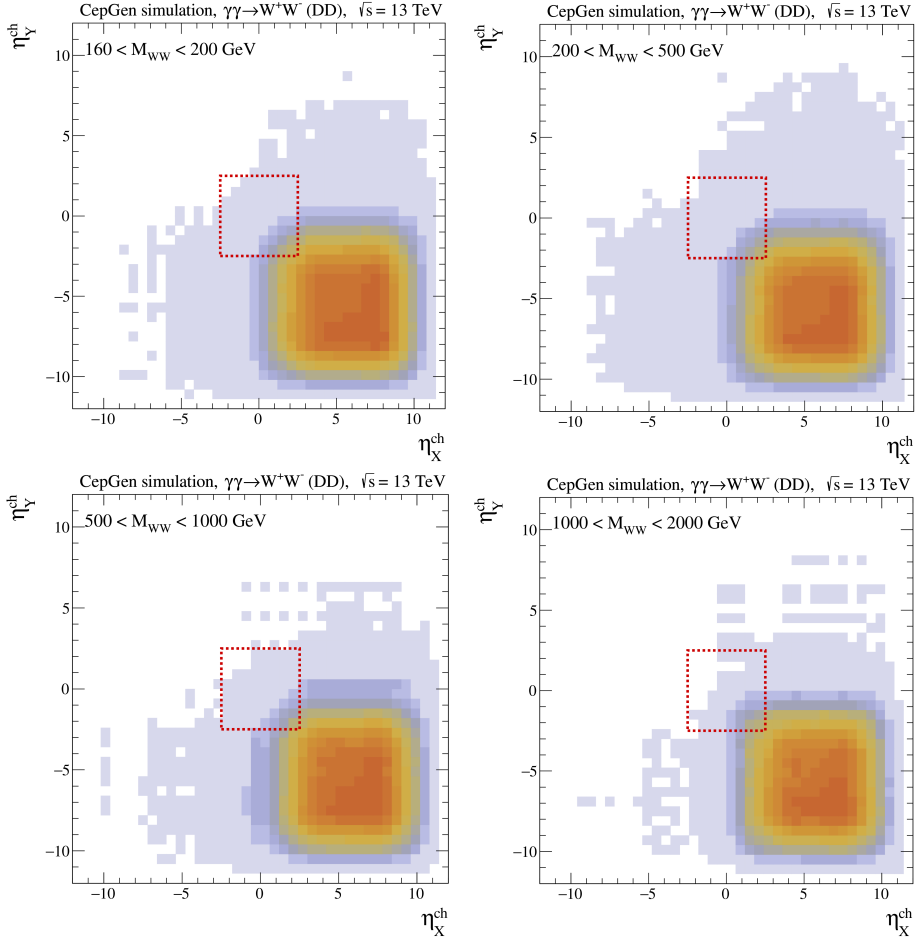


Fig. 4. Two-dimensional $(\eta_X^{\text{ch}}, \eta_Y^{\text{ch}})$ distribution for four different windows of M_{WW} : $(2M_W, 200 \text{ GeV})$, $(200, 500 \text{ GeV})$, $(500, 1000 \text{ GeV})$, $(1000, 2000 \text{ GeV})$. The square shows pseudorapidity coverage of ATLAS or CMS inner tracker.

We quantify this effect, see Table I, by showing average remnant rapidity gap factors for different ranges of M_{WW} masses. There we observe a rather mild dependence. The remnant rapidity gap survival factor at fixed η_{cut} becomes larger at higher collision energies.

In Fig. 5, we show the distribution in η_{cut} for the double dissociation process. We predict a strong dependence on η_{cut} . It would be valuable to perform experimental measurements with different η_{cut} .

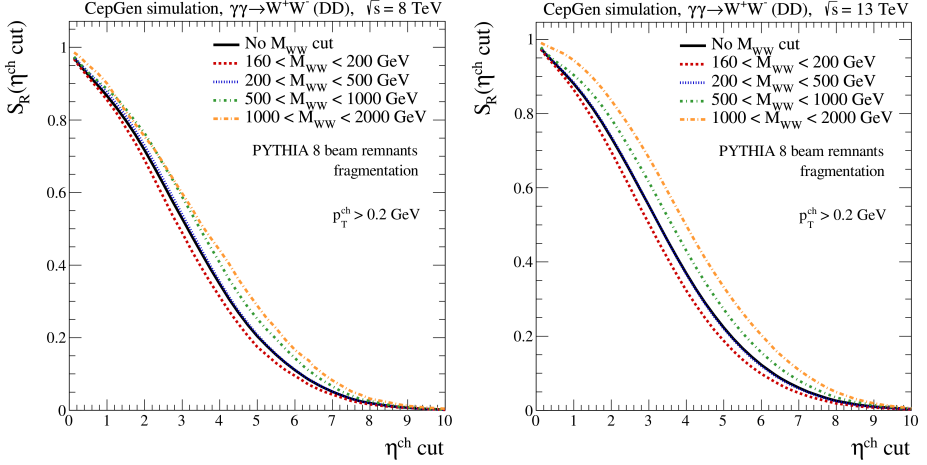


Fig. 5. Gap survival factor for double dissociation as a function of the size of the pseudorapidity veto applied on charged particles emitted from proton remnants, for the diboson mass bins defined in the text and in the figures for $\sqrt{s} = 8$ TeV (left) and 13 TeV (right).

4. Results for $t\bar{t}$ pairs production

In Table II, we show integrated cross sections for each of the categories of $\gamma\gamma$ processes shown in Fig. 1. We observe the following hierarchy as far as the integrated cross section is considered:

$$\sigma_{t\bar{t}}^{\text{el-el}} < \sigma_{t\bar{t}}^{\text{in-el}} = \sigma_{t\bar{t}}^{\text{el-in}} < \sigma_{t\bar{t}}^{\text{in-in}}. \quad (7)$$

The summed inclusive cross section at $\sqrt{s} = 13$ TeV is 2.36 fb. This is a rather small number in comparison with other inclusive production mechanisms. In the right panel of Table II, we show results when a rapidity gap¹

TABLE II

Cross section in fb at $\sqrt{s} = 13$ TeV for different components (left column) and the same when the extra condition on the outgoing jet $|y_{\text{jet}}| > 2.5$ is imposed.

Contribution	No cuts	y_{jet} cut
Elastic–elastic	0.292	0.292
Elastic–inelastic	0.544	0.439
Inelastic–elastic	0.983	0.622
All contributions	2.36	1.79

¹ That means no additional particle production except t or \bar{t} .

in the central region, for $-2.5 < y < 2.5$, is required in addition. In principle, imposing this condition requires modelling of the full final state, as we did for the case of W^+W^- production. As in each event we have the full four-momentum of the virtual photon(s), as well as the invariant masses of the proton remnants, the four-momenta of the recoiling jet(s) can be reconstructed. To a good accuracy, the rapidity gap condition is equivalent to require that the recoiling jets fulfill $|y_{\text{jet}}| > 2.5$.

The same is true for the distribution in $t\bar{t}$ invariant mass (see the left panel of Fig. 6). The distributions are almost identical and differ only by normalisation. In the right panel of Fig. 6, we show similar results when conditions on outgoing light quark/antiquark jets are imposed. The extra condition leads to a lowering of the cross section with only very small modification of the shape of the $M_{t\bar{t}}$ distribution.

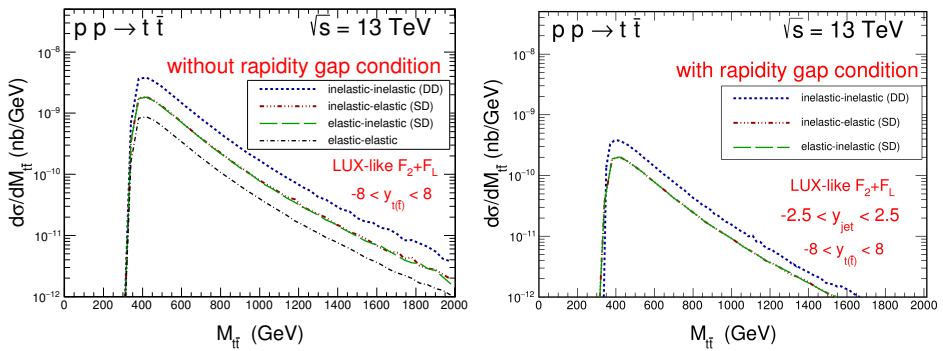


Fig. 6. $t\bar{t}$ invariant mass distribution for different components defined in the figure. The left panel is without imposing the condition on the struck quark/antiquark and the right panel includes the condition.

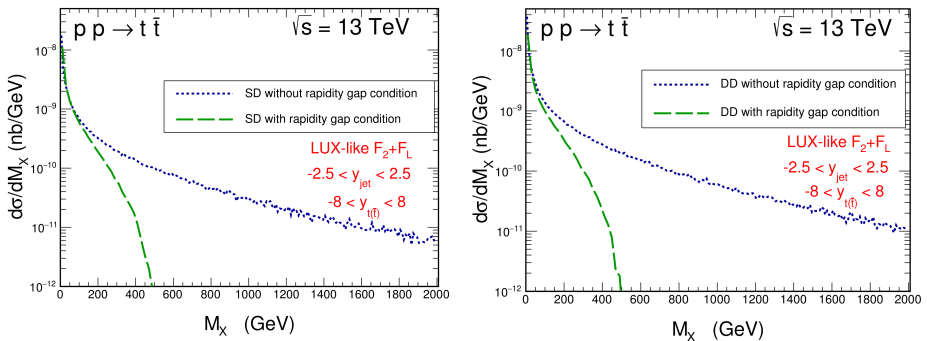


Fig. 7. Distribution in the mass of the dissociated system for single dissociation (left) and double dissociation (right). We show the result without and with the rapidity gap condition.

In addition, in Fig. 7 we show distributions in outgoing proton remnant masses M_X and/or M_Y . Similar shapes are observed for single dissociative and double dissociative processes. Population of large M_X or M_Y masses is associated with the emissions of jets visible in central detectors (*i.e.* with $-2.5 < y_{\text{jet}} < 2.5$). We show the distribution in the remnant mass M_X separately for the single dissociation (left) and double dissociation (right). As can be seen, the rapidity gap requirement introduces a rather sharp cut-off in the large-mass tail of the M_X -distribution.

In Fig. 8, we show distributions in M_X for a fixed M_Y (left panel) and in M_Y for a fixed M_X (right panel). The distributions are arbitrarily normalized to the same integral. All the distributions coincide.

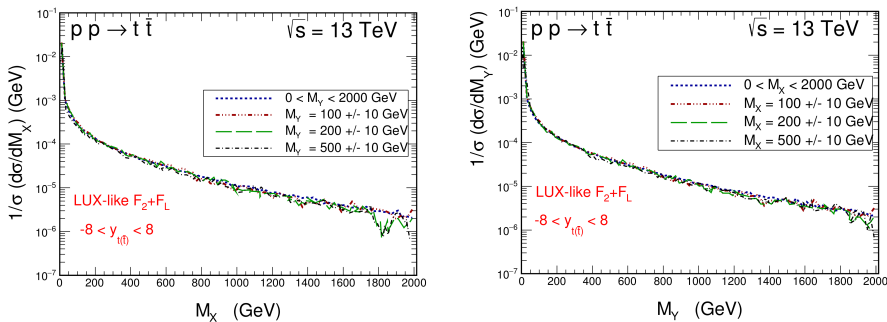


Fig. 8. Distribution in M_X for different windows of M_Y (left), and as a function of M_Y for different windows of M_X (right).

Finally, in Fig. 9 we show our results for $pp \rightarrow \gamma\gamma \rightarrow t\bar{t}$ processes. The gap survival factor fullfills the relation $S_{R,DD} < S_{R,SD}$. We have checked that the factorisation $S_{R,DD} = S_{R,SD}^2$ holds to very good accuracy.

5. Conclusions

In this presentation, we have discussed the quantity called remnant gap survival factor for the $pp \rightarrow W^+W^-$ and $pp \rightarrow t\bar{t}$ reactions initiated via photon–photon fusion. We use our formalism developed for the inclusive case [13] which includes transverse momenta of incoming photons. The partonic formalism has been supplemented by including remnant fragmentation that can spoil the rapidity gap usually used to select the subprocess of interest. We quantify this effect by defining the remnant gap survival factor which, in general, depends on the reaction, kinematic variables and details of the experimental set-ups. We have found that the hadronisation only mildly modifies the gap survival factor calculated on the parton level. We find different values for double and single dissociative processes. In general, $S_{R,DD} < S_{R,SD}$ and $S_{R,DD} \approx S_{R,SD}^2$.

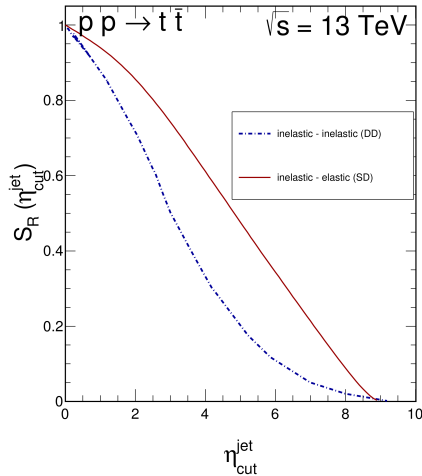


Fig. 9. Gap survival factor for single and double dissociation as a function of the size of the pseudorapidity veto applied on the recoiling jet emitted from proton remnants.

The cross sections for production of $t\bar{t}$ pairs via $\gamma^*\gamma^*$ fusion summed over the different categories of processes is about 2.36 fb (full phase space), *i.e.*, rather small compared to the standard inclusive $t\bar{t}$ cross section (of the order of nb). Our results imply that for the production of such heavy objects as t quark and \bar{t} antiquark, the virtuality of the photons attached to the dissociative system is very large ($Q^2 < 10^4 \text{ GeV}^2$).

REFERENCES

- [1] CMS Collaboration (S. Chatrchyan *et al.*), *J. High Energy Phys.* **1201**, 052 (2012), [arXiv:1111.5536 \[hep-ex\]](#).
- [2] CMS Collaboration (S. Chatrchyan *et al.*), *J. High Energy Phys.* **1211**, 080 (2012), [arXiv:1209.1666 \[hep-ex\]](#).
- [3] ATLAS Collaboration (G. Aad *et al.*), *Phys. Lett. B* **749**, 242 (2015), [arXiv:1506.07098 \[hep-ex\]](#).
- [4] CMS and TOTEM collaborations (A.M. Sirunyan *et al.*), *J. High Energy Phys.* **1807**, 153 (2018), [arXiv:1803.04496 \[hep-ex\]](#).
- [5] ATLAS Collaboration (M. Aaboud *et al.*), *Phys. Lett. B* **777**, 303 (2018), [arXiv:1708.04053 \[hep-ex\]](#).
- [6] CMS Collaboration (V. Khachatryan *et al.*), *J. High Energy Phys.* **1608**, 119 (2016), [arXiv:1604.04464 \[hep-ex\]](#).
- [7] ATLAS Collaboration (M. Aaboud *et al.*), *Phys. Rev. D* **94**, 032011 (2016), [arXiv:1607.03745 \[hep-ex\]](#).

- [8] E. Chapon, C. Royon, O. Kepka, *Phys. Rev. D* **81**, 074003 (2010), [arXiv:0912.5161 \[hep-ph\]](#).
- [9] T. Pierzchała, K. Piotrkowski, *Nucl. Phys. Proc. Suppl.* **179**, 257 (2008), [arXiv:0807.1121 \[hep-ph\]](#).
- [10] G.G. da Silveira *et al.*, *J. High Energy Phys.* **1502**, 159 (2015), [arXiv:1409.1541 \[hep-ph\]](#).
- [11] M. Łuszczak, W. Schäfer, A. Szczurek, *Phys. Rev. D* **93**, 074018 (2016), [arXiv:1510.00294 \[hep-ph\]](#).
- [12] M. Łuszczak, A. Szczurek, C. Royon, *J. High Energy Phys.* **1502**, 098 (2015), [arXiv:1409.1803 \[hep-ph\]](#).
- [13] M. Łuszczak, W. Schäfer, A. Szczurek, *J. High Energy Phys.* **1805**, 064 (2018), [arXiv:1802.03244 \[hep-ph\]](#).
- [14] L. Forthomme, M. Łuszczak, W. Schäfer, A. Szczurek, *Phys. Lett. B* **789**, 300 (2019), [arXiv:1805.07124 \[hep-ph\]](#).
- [15] M. Łuszczak, L. Forthomme, W. Schäfer, A. Szczurek, *J. High Energy Phys.* **1902**, 100 (2019), [arXiv:1810.12432 \[hep-ph\]](#).